Journal of Materials Chemistry A

PAPER

View Article Online
View Journal | View Issue



Cite this: J. Mater. Chem. A, 2014, 2, 4256

# $MnO_2$ decorated graphene nanoribbons with superior permittivity and excellent microwave shielding properties†

Tejendra K. Gupta,[a] Bhanu P. Singh,*[a] Vidya Nand Singh,[b] Satish Teotia,[a] Avanish Pratap Singh,[c] Indu Elizabeth,[a] Sanjay R. Dhakate,[a] S. K. Dhawan[c] and R. B. Mathur[a]

Received 23rd November 2013
Accepted 19th December 2013

DOI: 10.1039/c3ta14854h

www.rsc.org/MaterialsA

Microwave shielding properties of chemically synthesized $MnO_2$ decorated graphene nanoribbons (GNRs) are reported for the first time. The nature of $MnO_2$ decoration on the GNRs has been investigated using scanning electron microscopy, X-ray diffraction, Raman spectroscopy and high resolution transmission electron microscopy. The electromagnetic interference (EMI) shielding effectiveness of this material was investigated in the microwave region (Ku-band, 12.4–18 GHz). The presence of $MnO_2$ on GNR enhances the interfacial polarization, multiple scattering, natural resonances and the effective anisotropy energy, which leads to absorption dominated high shielding effectiveness of −57 dB (blocking >99.9999% radiation) by a 3 mm thick sample. Dielectric attributes ($\varepsilon'$ and $\varepsilon''$) were evaluated to understand the mechanism of the excellent shielding effectiveness. The material will be an excellent choice for radar absorbing applications.

## 1. Introduction

Electromagnetic (EM) interference shielding materials are currently in high demand (for both commercial and defense purposes) because of electromagnetic pollution which is generated due to extensive use of electrical and electronic equipment. EM radiation produced from an external source can disturb electrical circuits, cell phones, televisions, satellite communications, global positioning systems (GPS), *etc.* The disturbances across communication channels, automation and process control lead to the loss of precious time, energy, resources and even life. Therefore, shielding must be provided to protect today's society from electromagnetic pollution. In general, there are two practical ways for shielding against electromagnetic interference (EMI): the first is to protect certain components from the radiation by reflecting or absorbing the waves; another is to reduce the reflection and increase the absorption by incorporating dielectric or magnetic particles into it.

In the present study, we focus on the second type of shielding, called absorption dominated microwave shielding. The complex dielectric permittivity is an important parameter for describing the properties of absorption dominated microwave shielding or radar absorbing materials (RAM). Excellent dielectric properties are needed for making good RAM. Therefore, lightweight EMI shielding materials[1–3] are sought in order to shield the workspace and environment from incoming radiation from computers and telecommunications as well as for protection of sensitive circuits. Previously, metal based microwave shielding materials were widely explored and utilized but the high specific gravity, corrosion proneness and cumbersome processing methods made these materials unsuitable for both the researchers and users. Furthermore, metals mainly reflect the radiation and cannot be used for applications where absorption is mandatory. Nowadays, microwave shielding materials[4] with comparatively light weight, good flexibility and strong absorption in the gigahertz range are in high demand. Recently, carbon nanotubes (CNTs),[5] magnetic-particle-doped CNTs and nanostructured ZnO were intensively investigated and found to be promising shielding materials. Liu *et al.*[6] achieved a maximum absorption value of −22 dB at 8.8 GHz by 5 wt% single-walled carbon nanotubes (SWCNTs) loaded polyurethane composites. Fan *et al.*[7] reported a maximum absorption of about 24.3 dB at 15.3 GHZ by 8 wt% multi-walled carbon nanotubes (MWCNTs) loaded polymer (or varnish) composites. Singh *et al.*[8] reported a maximum shielding effectiveness due to absorption of −53 dB in the X-band (8.2–12.4 GHz) by 20.4 wt% MWCNTs loaded epoxy composites. Che *et al.*[9] have observed the microwave absorption of about −25 dB at 11 GHz by Fe–CNTs–epoxy composites. However, the complex fabrication process of CNTs

[a]Physics and Engineering of Carbon, Division of Materials Physics and Engineering, CSIR-National Physical Laboratory, New Delhi, 110012, India. E-mail: bps@mail.nplindia.org; Fax: +91-11-45609310; Tel: +91-11-45608460

[b]Electron and Ion Microscopy Section, CSIR-National Physical Laboratory, New Delhi, 110012, India

[c]Polymeric and Soft Materials Section, CSIR-National Physical Laboratory, New Delhi, 110012, India

† Electronic supplementary information (ESI) available. See DOI: 10.1039/c3ta14854h

or magnetic-particle-doped CNTs is a challenging task (for using such absorbing nanocomposites in practical applications). Therefore, there is a need to look for new materials with relatively light weight, good flexibility, long lasting and especially exceptional microwave shielding properties.

Nanoscale materials based on single-layered 2-D graphene sheets have recently attracted great interest due to their many extraordinary properties.[10] At present, carbon based composite materials employing CNTs are dominating the research and application fields. But the poor dispersion of CNTs due to bundling, the presence of impurities, lack of interfacial adhesion with other materials and high cost of production have marred their applications. It has been proposed that these issues could be reduced by incorporating graphene sheets into composite materials.[11,12] Graphene nanoribbons (GNRs) have also been found an important material in the carbon allotrope family. GNRs have been synthesized by different routes previously.[13–18]

On the other hand, manganese oxide ($MnO_2$) offers a new path for the development of advance microwave shielding materials because of its low cost and environment friendly nature. It is well known that the pseudo-capacitive reaction of $MnO_2$ is a surface reaction and therefore only a very thin layer of $MnO_2$ is sufficient for high microwave shielding.[19] Thus, ultra-thin $MnO_2$ can deliver very high microwave shielding.

There are only few reports on using $MnO_2$ as a microwave shielding material. Duan *et al.*[20] studied the microwave absorbing properties of α-$MnO_2$–carbon black composites and showed that these composites can absorb microwaves in a wide band range at about 8.7 GHz with lower than −10 dB (90% absorption) due to dielectric loss. Microwave absorption properties of $MnO_2$ composites were also studied by Guan *et al.*[21] In their study, $MnO_2$–$SiO_2$–PVA composites had the strongest absorbing peak of about 25 dB at 8.5 GHz for 30 vol% $MnO_2$.

In the present study, we demonstrate the successful preparation of $MnO_2$ decorated GNRs *via* a chemical method in the presence of concentrated sulfuric acid which plays an important role in increasing the interlayer distance of graphene layers. The EMI shielding and dielectric properties of $MnO_2$ decorated GNRs are studied and it is observed that the incorporation of $MnO_2$ improves the electromagnetic absorption properties which is due to the enhancement of dielectric loss. We also explored the effect of varying thickness of the composites on the EMI shielding performance.

# 2. Experimental

## 2.1. Materials

Natural graphite with purity > 99% and BS mesh 500 was purchased from Pune Carbon, Pune, India. $KMnO_4$ (purity > 99%) and $H_2SO_4$ (purity > 98%) were purchased from Qualigens fine chemicals, Mumbai, India and RANKEM, New Delhi, India, respectively.

## 2.2. Process for decoration of GNRs with $MnO_2$

In a typical procedure as shown in Scheme 1, graphite flakes (50 mg) were mixed with $KMnO_4$ crystallites (300 mg) using planetary ball milling (2 h, 250 rpm) and a powder mixture was obtained. This mixture was suspended in 50 ml distilled water and stirred using a magnetic stirrer (speed 600 rpm) at room temperature for 12 h. 5 ml of concentrated $H_2SO_4$ was introduced into the solution while continuing stirring (at 80 °C) for an additional 2 h. The reaction mixture was removed from the heat source, and poured into 500 ml distilled water to cool it down and dilute it. The solution was then filtered using a 0.22 μm pore size Whatman filter followed by several washings with de-ionized water till the pH became neutral.

## 2.3. Characterization

Surface morphology of $MnO_2$ decorated GNRs was investigated using SEM (Leo 440S, UK) and microstructural properties were investigated using HRTEM (Technai G30-stwin, 300 kV instrument). Raman studies were carried out using a Renishaw inVia reflex Raman spectrometer, UK with an excitation source of 514.5 nm. The XRD patterns were recorded using a Bruker D8 Advance X-ray diffractometer in the diffraction ($2\theta$) range of 10–70° (slit width of 0.1 mm) using the Cu Kα line ($\lambda = 1.5405$ A) as radiation source. EMI shielding effectiveness (SE) and electromagnetic attributes (real and imaginary permittivity) were measured using a vector network analyzer (VNA E8263B Agilent Technologies) by placing pellet having dimensions 15.8 × 7.9 $mm^2$ inside a copper sample holder connected between the wave-guide flanges of the network analyzer in the Ku-band (12.4–18.0 GHz) waveguide. These obtained complex parameters were estimated from experimental scattering parameters ($S_{11}$ and $S_{21}$) by standard Nicholson–Ross and Weir theoretical calculations.[22] Furthermore, reflection and transmission coefficients were also evaluated using scattering parameters:, $R = |S_{11}|^2 = |S_{22}|^2$ and $T = |S_{21}|^2 = |S_{12}|^2$. The absorbance was calculated as $A = 1 - R - T$.

# 3. Results and discussion

## 3.1. Morphological and structural characterizations

The surface morphology of the as-synthesized $MnO_2$ decorated GNR was studied using SEM. In Fig. 1(a), some layered structures are observed in $MnO_2$ decorated GNRs, and the GNRs are not clearly visible due to the coating of $MnO_2$ over the surface of GNRs. EDX analysis (Fig. 1(b)) shows the presence of Mn (53%),

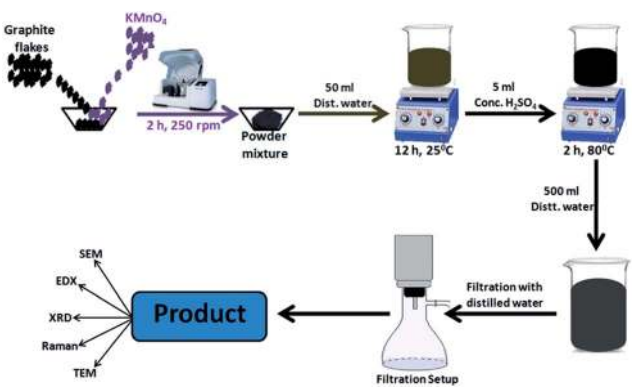


Scheme 1 Synthesis process of decoration of GNRs with $MnO_2$.

O (40%), and C (7%). XRD analysis was used to determine the structure of the hybrid. The peak at a $2\theta$ value of 12.73° in Fig. 1(c) is due to the (110) plane of $\alpha$-$MnO_2$. Other peaks are assigned to the tetragonal phase of $\alpha$-$MnO_2$ (JCPDS 44-0141) indicating better crystallinity in strong acidic medium.[23,24] Moreover, a low intensity peak corresponding to the (002) plane (inset of Fig. 1(c)) of graphitic structure was observed in $MnO_2$ decorated GNR samples. This might be due to the presence of excess $MnO_2$ which prevented the stacking of graphene sheets over each other to form crystalline structures.[25] This is evident from the EDX results which show that the carbon content in $MnO_2$ decorated GNRs is only 7 wt%.

Fig. 1(d) shows the room temperature Raman spectrum of $MnO_2$ decorated GNRs. The Raman spectrum was recorded using a low laser power of 5 mW in order to avoid any decomposition of the sample. The Raman spectrum of $MnO_2$ decorated GNRs is dominated by a sharp and strong band at approximately 645 $cm^{-1}$ with a shoulder at 576 $cm^{-1}$ which can be assigned to $\alpha$-$MnO_2$. The Raman band at 645 $cm^{-1}$ of the $A_{1g}$ mode is attributed to symmetric Mn–O stretching vibrations of

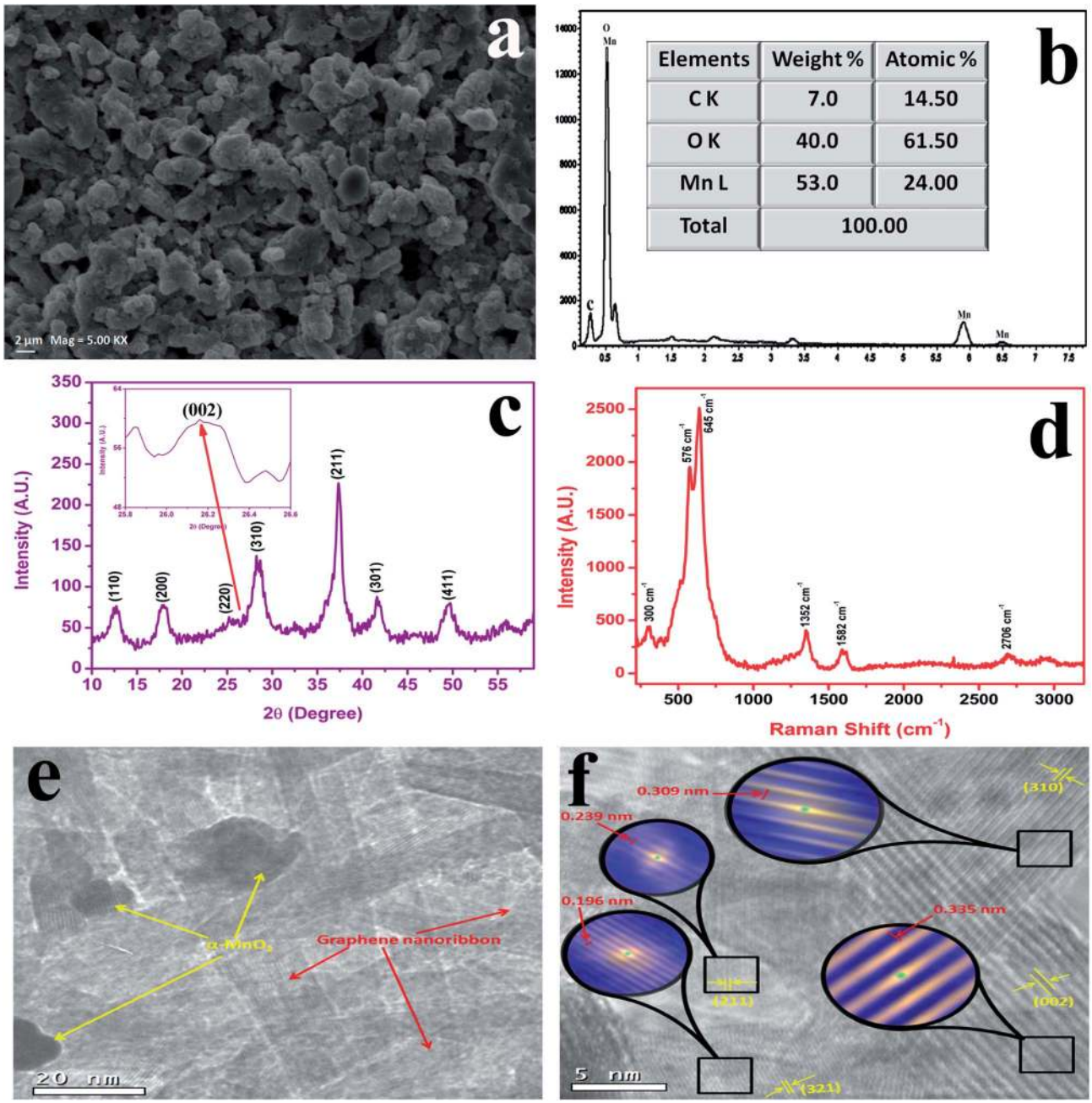


Fig. 1 (a) SEM image, (b) EDX results, (c) XRD pattern, (d) Raman spectrum of $MnO_2$ decorated GNRs, (e) TEM image showing the presence of $MnO_2$ (yellow arrows) on the surface of GNR (red arrows) and (f) showing the inter-planar spacing (yellow lines) and an enlarged view of the lattice fringes (black circles).

 

tetragonal $MnO_2$. The shoulder peak at 576 $cm^{-1}$ of the $F_{2g}$ mode is not well distinguishable because of its low intensity. This shoulder peak is closely related to the oxidation state of manganese and appears due to the vibration of Mn–O bonds.[26,27]

The two most intense features of the Raman spectrum are the presence of a G peak at ~1582 $cm^{-1}$ and a 2D peak at ~2706 $cm^{-1}$, as usually observed in graphitic structures.[28] The G and D bands are due to the doubly degenerate zone centre $E_{2g}$ mode[29] at ~1582 $cm^{-1}$ and the breathing modes of six atom rings which appears at 1352 $cm^{-1}$ due to the presence of defects in the graphite,[28] respectively. The 2D peak is due to the second order defects. The 2D peak in bulk graphite consists of two components, $2D_1$ (shoulder) and $2D_2$,[29,30] with heights roughly 1/4 and 1/2 of the height of the G peak, respectively. But the Raman spectrum of graphene has a single sharp 2D peak. The number of layers in graphene is estimated based on the intensity of the 2D peak. In the above figure, the D, G and 2D peak position values satisfy the criteria for the presence of graphene type structure in the $MnO_2$ decorated GNRs.

The TEM micrograph (Fig. 1(e)) shows that $MnO_2$ nanoparticles are spherical in shape (indicated by yellow arrows) and the particle size is in the range of 10–20 nm. They cover the surface of GNRs. The ribbon-like structure (red arrows) is a clear indication of the presence of nanocrystalline GNRs. The HRTEM micrograph (Fig. 1(f)) shows well-defined inter-planar spacings of 0.309 nm, 0.239 nm and 0.196 nm, which correspond to the (310), (211) and (321) planes of $\alpha$-$MnO_2$. The inter-planar spacing of 0.354 nm corresponds to the (002) plane of graphene. The detailed microscopic evidence of $MnO_2$ decoration on GNRs is shown in HRTEM images (Fig. S1, ESI SP1†). All the above characterizations confirm the decoration of $MnO_2$ on GNRs.

### 3.2. Proposed reaction mechanism

Based on the above results, a mechanism for the formation of $MnO_2$ decorated GNRs is proposed and the scheme is shown in Fig. 2. In the preliminary stage, when a large amount of $KMnO_4$ is mixed with graphite under neutral conditions, it acts as a 'weak oxidizing agent' due to the much lower positive potential of $KMnO_4$ in a neutral medium than that in an acidic medium.[31,32] During the slow oxidation process, oxygen-containing groups would attach themselves spontaneously on the graphite sheets.

In the next stage, when a small amount of $H_2SO_4$ is introduced into the system, $KMnO_4$ in the acidic medium oxidizes graphite faster, which links the oxidized sites to curved epoxy chains.[33] Step by step, $MnO_4^-$ ions are absorbed and precipitated on the oxidized location through the interactions between remaining $KMnO_4$ and hydroxyl groups. When the solution mixture is heated, oxidation of the graphite layers is significantly enhanced. Intercalation of $SO_4^{2-}$ increases the distance between graphite layers. Insoluble $MnO_2$ precipitates on the expanded graphite and cannot be washed away.

### 3.3. Microwave shielding effectiveness

The EMI SE is defined as the logarithmic ratio of incoming power ($P_i$) to outgoing power ($P_t$) of radiation. In general, the efficiency of any shielding material is expressed in decibels (dB). For a higher decibel level of EMI shielding effectiveness, less energy must be transmitted through the shield. It depends upon the following three factors:[3,34]

(a) *absorption*: the wave is absorbed in the shielding material,

(b) *reflection*: the wave is reflected from the front surface of the shielding material,

(c) *multiple reflections*: reflections of the waves from various interfaces

Therefore, the total EMI shielding effectiveness can be expressed as[1,2,8,35–37]

$$SE_T\ (dB) = SE_A + SE_R + SE_M = 10 \log_{10}\left(\frac{P_t}{P_i}\right) \quad (1)$$

As $P_t$ is always less than $P_i$, the shielding effectiveness is a negative quantity. When the total EMI shielding effectiveness of the material is more than −10 dB, then loss due to multiple reflections ($SE_M$) becomes negligible and can be neglected.[34,38,39] Thus, the total shielding effectiveness ($SE_T$) can be expressed as

$$SE_T\ (dB) = SE_A + SE_R \quad (2)$$

A schematic diagram showing the interaction of electromagnetic waves with $MnO_2$ decorated GNRs is shown in Fig. 3. Reflection (R), absorption (A) and multiple internal reflections (MIR) which contribute towards the overall attenuation (with $SE_R$, $SE_A$ and $SE_M$ components, respectively) are shown. When the electromagnetic wave falls on $MnO_2$ decorated GNRs, the dominant loss of the incident electromagnetic wave is through absorption. The energy is consumed mainly due to dielectric loss (because of the presence of a large amount of dielectric material, $\alpha$-$MnO_2$). A small part of the incident electromagnetic wave is reflected from the front and back interfaces of the material.

Microwave shielding materials having strong absorption, low density, and good physical and chemical stability are in high demand. Conventional microwave shielding materials (metals and magnetic materials) have limited practical applications due to their high specific gravity, difficulty in formulation and lack of proper response to gigahertz frequencies.[40]

The frequency dependence of microwave absorption is a key criterion in selecting materials for EMI shielding applications. $MnO_2$ and graphene were selected in our experiments because of their high dielectric and absorption properties, respectively. Microwave shielding properties of these $MnO_2$ decorated GNRs were examined by making rectangular pellets of different thicknesses (0.5 mm, 1.0 mm, 1.5 mm, 2.0 mm, 2.5 mm and 3.0 mm). The pellets were placed in the Ku-band sample holder and shielding effectiveness was examined in the frequency range of 12.4–18.0 GHz. The plots of microwave shielding effectiveness *versus* frequency for $MnO_2$ decorated GNRs having six different thicknesses are shown in Fig. 4. The value of $SE_T$ is −11 dB for the sample having a thickness of 0.5 mm and it reaches −57 dB for the 3.0 mm thick sample (Fig. 4(a)). The terms $SE_R$ and $SE_A$ show the shielding contributions due to reflection and absorption, respectively and can be expressed mathematically as:[2,34]

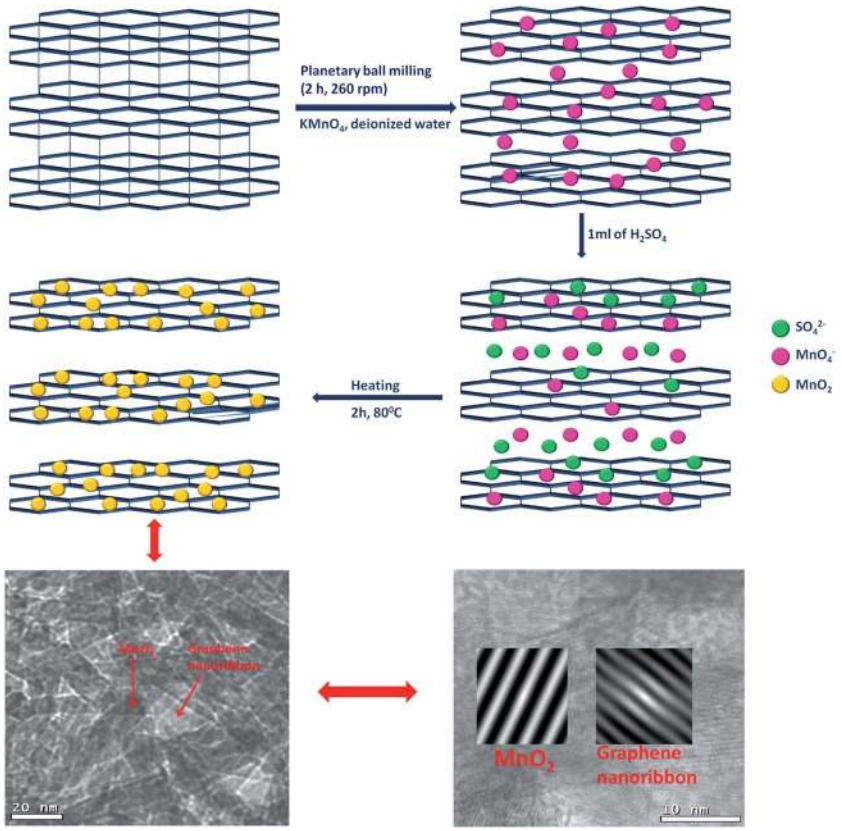


Fig. 2 Proposed mechanism for the formation of $MnO_2$/graphene nanoribbons.

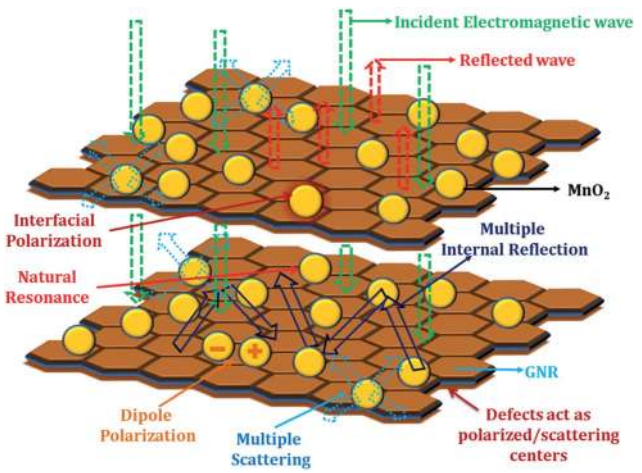


Fig. 3 Schematic presentation of possible microwave shielding mechanism in $MnO_2$ decorated GNRs.

$$SE_R\ (dB) = 108 + \log_{10}\left(\frac{\sigma}{f\mu}\right) \quad (3)$$

$$SE_A\ (dB) = -10\log_{10}\left(\frac{P_t}{P_i}\right) = -8.68\{t/\delta\} = -8.68\alpha t \quad (4)$$

where $\alpha$ is the attenuation coefficient which describes the extent to which the intensity of an electromagnetic wave is reduced when it passes through a specific material.

$$\alpha = \frac{4\pi n}{\lambda_0} \quad (5)$$

where $n$ is the refractive index of the material and $\lambda_0$ is the wavelength in vacuum. Refractive index ($n$) is defined by the following relation:

$$n = (\varepsilon_r\mu_r)^{1/2} \quad (6)$$

where $\varepsilon_r$ and $\mu_r$ are the relative permittivity and permeability, respectively.

For non-magnetic materials $\mu_r$ is very close to 1.[41] Therefore, $n = (\varepsilon_r)^{1/2}$ and we know that for a medium, $\varepsilon_r$ is equal to $\varepsilon'$. Therefore,

$$n = (\varepsilon')^{1/2} \quad (7)$$

where $\varepsilon'$ is the real part of permittivity.

Wavelength in vacuum ($\lambda_0$) is equal to $\lambda_0 = 2\pi c/\omega$ because $\omega = 2\pi n = 2\pi c/\lambda_0$, where $c$ is the velocity of light and is described as:

$$c = (\varepsilon_r\mu_r)^{-1/2} \quad (8)$$

Therefore,

$$\lambda_0 = \frac{2\pi}{\omega(\varepsilon_r\mu_r)^{1/2}} \quad (9)$$

For non-magnetic materials, $\mu_r = 1$. Thus, high permittivity is very important for the enhancement of $SE_A$ and suppressing

 

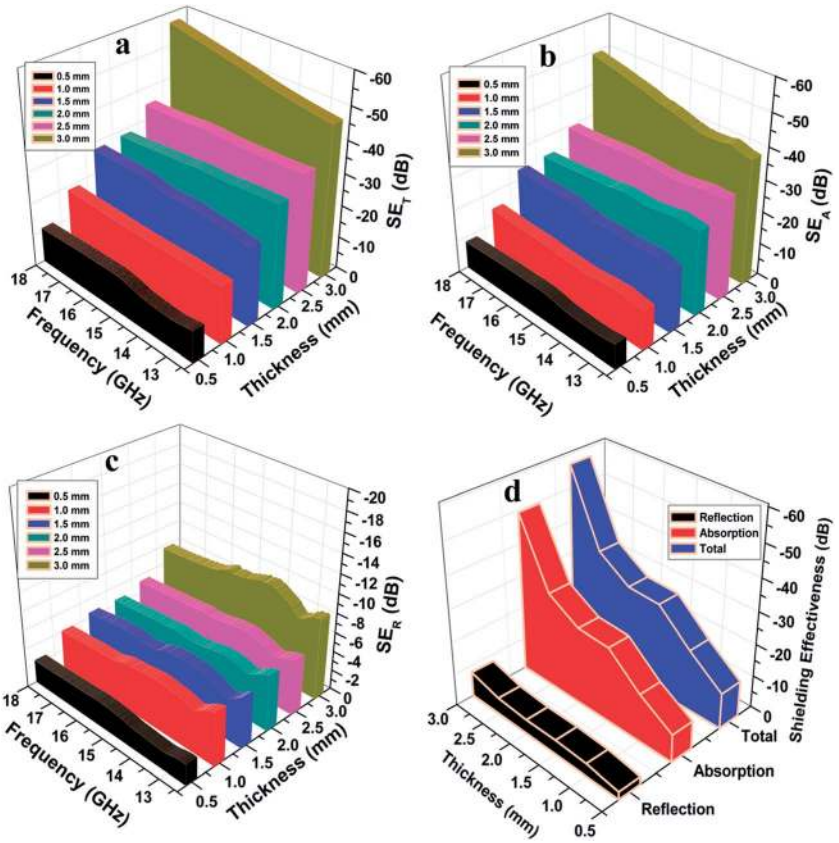


Fig. 4 Variation of (a) $SE_T$, (b) $SE_A$, (c) $SE_R$ with frequency for different thicknesses of $MnO_2$ decorated GNRs and (d) $SE_T$, $SE_A$ and $SE_R$ for different thicknesses of $MnO_2$ decorated GNRs at 18.0 GHz.

$SE_R$, respectively. Thus, the incorporation of very high permittivity material, $MnO_2$ nanoparticles, in GNRs enhanced the overall shielding effectiveness.

Fig. 4(b) shows that $SE_A$ increases with increase in thickness and the value increased from −8.63 dB for the 0.5 mm thick sample to −49.34 dB for the 3.0 mm thick sample. This trend in reflection loss ($SE_R$) is very small (Fig. 4(c)) where it varies from −2.4 dB for 0.5 mm to −7.7 dB for the 3.0 mm thick sample. Fig. 4(d) shows the overall changes in % attenuation with thickness, in which changes in reflection loss with increasing thickness are very small as compared to absorption.

In the study of Hailong *et al.*,[42] graphene was used as a microwave absorbing material and it showed a microwave absorption of −11 dB for a sample having a thickness of 4.0 mm in the 2.0–18.0 GHz frequency range. In another study, Wang *et al.*[43] reported 6.9 dB microwave absorption at 7 GHz using chemically reduced graphene oxide. Therefore an attempt has been made to improve $SE_A$ by incorporating a high dielectric material ($MnO_2$ nanoparticles).

According to the electromagnetic theory, dielectric losses in a material occur because of complex phenomena such as natural resonances, dipolar relaxation, electronic polarization and its relaxation, and the unique structure of the material. In $MnO_2$ decorated GNRs, $MnO_2$ acts as a polarized centre in the presence of microwaves which gives rise to better microwave shielding due to absorption. The relative complex permittivity ($\varepsilon^* = \varepsilon' - i\varepsilon''$) (at room temperature) has been measured for investigating the microwave shielding properties of $MnO_2$ decorated GNRs. The real part of permittivity ($\varepsilon'$) is mainly associated with the amount of polarization in the material and is related to the storage of electrical energy, whereas the imaginary part of permittivity ($\varepsilon''$) is a measure of loss in energy. Fig. 5(a) shows the real ($\varepsilon'$) and imaginary ($\varepsilon''$) parts of the relative complex permittivity of $MnO_2$ decorated GNRs in the frequency range of 12.4–18 GHz. It can be observed from Fig. 5(a) that $\varepsilon'$ shows the highest value of 335 at 12.7 GHz and it decreases with fluctuations (from 320 to 223) in the 12.4–18.0 GHz range, similar to earlier reports.[36,43,44] The $\varepsilon''$ value is lower than $\varepsilon'$ and it fluctuates (from 173 to 100) in the 12.4–18.0 GHz range. The relatively high values of $\varepsilon''$ and tan $\delta_\varepsilon$ (Fig. 5(b)) show that α-$MnO_2$ decorated GNRs exhibit high dielectric losses. These dielectric losses are attributed to complex phenomena, such as: natural resonance, dominant electronic and dipolar polarization, interfacial polarization and associated relaxation phenomena.[36,45,46] The dielectric tangent loss (tan $\delta_\varepsilon = \varepsilon''/\varepsilon'$) based on the permittivity of the sample has also been evaluated and the values are in the range of 0.5 to 0.45 as shown in Fig. 5(b). This indicates higher absorption loss (−49.34 dB) which is equivalent to 99.9999% attenuation.

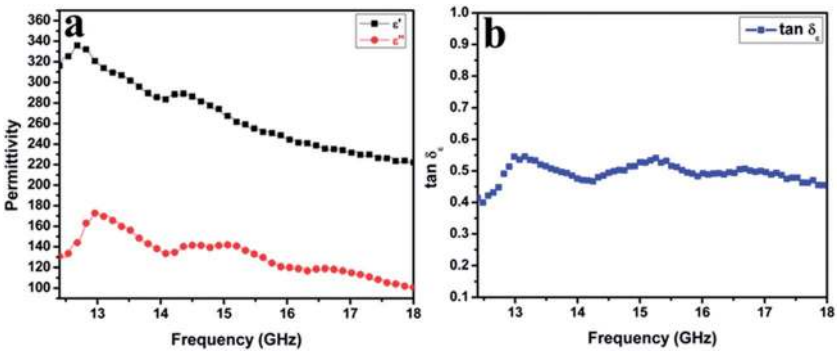


Fig. 5 Frequency dependence of (a) real and imaginary parts of permittivity and (b) corresponding dielectric tangent loss of $MnO_2$ decorated GNRs for a 3.0 mm thick sample.

Conventionally the relaxation process described by the Cole–Cole semicircles has an important effect on the permittivity behavior of microwave absorbing materials.

According to the Debye dipolar relaxation process,[43,47] the complex permittivity can be written as

$$(\varepsilon' - \varepsilon_\infty)^2 + (\varepsilon'')^2 = (\varepsilon_s - \varepsilon_\infty)^2 \quad (10)$$

where $\varepsilon_s$ and $\varepsilon_\infty$ are the static dielectric constant and the dielectric constant at infinite frequency, respectively. The $\varepsilon' - \varepsilon''$ curve of $MnO_2$ decorated GNRs is shown in Fig. 6. The Cole–Cole plot presents a clear segment of three semicircles. The result demonstrates that there are three dielectric relaxation processes in the $MnO_2$ decorated GNRs with each semicircle corresponding to one Debye relaxation process which enhances the dielectric properties of $MnO_2$ decorated GNRs. In $MnO_2$ decorated GNRs, the existence of interfaces between $MnO_2$–$MnO_2$, GNR–GNR and $MnO_2$–GNR gives rise to interfacial polarization or Maxwell–Wagner–Sillars polarization.

The phenomenon of interfacial and space charge relaxation appears because charge carriers are trapped at the interfaces of heterogeneous media. Evidently, the Cole–Cole semicircles are distorted which reveals that except for the dielectric relaxation, other phenomena such as conductance loss, interfacial polarization and oxygen defects contribute to the permittivity spectra. Therefore, in $MnO_2$ decorated GNRs, ternary dielectric relaxation, interfacial polarization and effective anisotropy energy are helpful in improving the level of impedance matching for the excellent microwave shielding due to absorption.

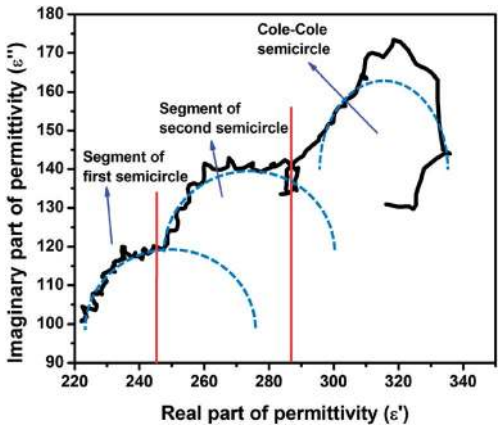


Fig. 6 Typical Cole–Cole plot of $MnO_2$ decorated GNRs.

## 4. Conclusion

$MnO_2$ decorated graphene nanoribbons (GNRs) have been synthesized by a chemical route which results in $MnO_2$ intercalated graphene. The material was further characterized using SEM, EDX, XRD, Raman and HRTEM. The results show that the existence of $MnO_2$ in GNRs effectively enhances the electronic polarization, interfacial polarization and anisotropy energy in the presence of microwaves. A maximum shielding effectiveness of −57 dB was achieved for a 3.0 mm thick sample and is mainly governed by absorption rather than reflection. Thus, inclusion of $MnO_2$ in GNRs is highly useful for better microwave absorption in Ku band (12.4–18 GHz) as compared to conventional materials. Additionally, the shielding effectiveness can easily be tailored by varying the thickness of the sample. It is believed that this kind of material will find applications in microwave absorbing area.

## Acknowledgements

The authors are grateful to the Director, CSIR-National Physical Laboratory, New Delhi for his kind support and encouragement. Authors also wish to thank Mr K. N. Sood and Mr Jai Tawale for SEM characterization. One of the authors (TKG) acknowledges CSIR, Govt of India for providing a Senior Research Fellowship (SRF).

## References

1 T. K. Gupta, B. P. Singh, S. Teotia, V. Katyal, S. R. Dhakate and R. B. Mathur, *J. Polym. Res.*, 2013, **20**, 1–7.
2 B. P. Singh, Prabha, P. Saini, T. Gupta, P. Garg, G. Kumar, I. Pande, S. Pande, R. K. Seth, S. K. Dhawan and R. B. Mathur, *J. Nanopart. Res.*, 2011, **13**, 7065–7074.
3 R. Kumar, S. R. Dhakate, T. Gupta, P. Saini, B. P. Singh and R. B. Mathur, *J. Mater. Chem. A*, 2013, **1**, 5727–5735.
4 V. M. Petrov and V. V. Gagulin, *Inorg. Mater.*, 2001, **37**, 93–98.

 

5 N. Li, Y. Huang, F. Du, X. He, X. Lin, H. Gao, Y. Ma, F. Li, Y. Chen and P. C. Eklund, *Nano Lett.*, 2006, **6**, 1141–1145.
6 Z. Liu, G. Bai, Y. Huang, F. Li, Y. Ma, T. Guo, X. He, X. Lin, H. Gao and Y. Chen, *J. Phys. Chem. C*, 2007, **111**, 13696–13700.
7 Z. Fan, G. Luo, Z. Zhang, L. Zhou and F. Wei, *Mater. Sci. Eng., B*, 2006, **132**, 85–89.
8 B. P. Singh, Prasanta, V. Choudhary, P. Saini, S. Pande, V. N. Singh and R. B. Mathur, *J. Nanopart. Res.*, 2013, **15**, 1–12.
9 R. C. Che, L. M. Peng, X. F. Duan, Q. Chen and X. L. Liang, *Adv. Mater.*, 2004, **16**, 401–405.
10 A. K. Geim and K. S. Novoselov, *Nat. Mater.*, 2007, **6**, 183–191.
11 S. Stankovich, D. A. Dikin, G. H. B. Dommett, K. M. Kohlhaas, E. J. Zimney, E. A. Stach, R. D. Piner, S. B. T. Nguyen and R. S. Ruoff, *Nature*, 2006, **442**, 282–286.
12 T. Ramanathan, A. A. Abdala, S. Stankovich, D. A. Dikin, M. Herrera-Alonso, R. D. Piner, D. H. Adamson, H. C. Schniepp, X. Chen, R. S. Ruoff, S. T. Nguyen, I. A. Aksay, R. K. Prud'Homme and L. C. Brinson, *Nat. Nanotechnol.*, 2008, **3**, 327–331.
13 L. Xie, H. Wang, C. Jin, X. Wang, L. Jiao, K. Suenaga and H. Dai, *J. Am. Chem. Soc.*, 2011, **133**, 10394–10397.
14 X. Li, X. Wang, L. Zhang, S. Lee and H. Dai, *Science*, 2008, **319**, 1229–1232.
15 L. Jiao, L. Zhang, X. Wang, G. Diankov and H. Dai, *Nature*, 2009, **458**, 877–880.
16 L. Jiao, L. Zhang, L. Ding, J. Liu and H. Dai, *Nano Res.*, 2010, **3**, 387–394.
17 L. Jiao, X. Wang, G. Diankov, H. Wang and H. Dai, *Nat. Nanotechnol.*, 2010, **5**, 321–325.
18 L. Jiao, L. Xie and H. Dai, *Nano Res.*, 2012, **5**, 292–296.
19 S. B. Ma, K. Y. Ahn, E. S. Lee, K. H. Oh and K. B. Kim, *Carbon*, 2007, **45**, 375–382.
20 Y. Duan, Y. Yang, M. He, S. Liu, X. Cui and H. Chen, *J. Phys. D: Appl. Phys.*, 2008, **41**, 125403.
21 H. Guan, S. Liu, Y. Zhao and Y. Duan, *J. Electron. Mater.*, 2006, **35**, 892–896.
22 A. M. Nicolson and G. F. Ross, *IEEE Trans. Instrum. Meas.*, 1970, **19**, 377–382.
23 J. Luo, H. T. Zhu, H. M. Fan, J. K. Liang, H. L. Shi, G. H. Rao, J. B. Li, Z. M. Du and Z. X. Shen, *J. Phys. Chem. C*, 2008, **112**, 12594–12598.
24 W. Xiao, D. Wang and X. W. Lou, *J. Phys. Chem. C*, 2010, **114**, 1694–1700.
25 J. Yan, Z. Fan, T. Wei, W. Qian, M. Zhang and F. Wei, *Carbon*, 2010, **48**, 3825–3833.
26 C. Julien, M. Massot, R. Baddour-Hadjean, S. Franger, S. Bach and J. P. Pereira-Ramos, *Solid State Ionics*, 2003, **159**, 345–356.
27 C. Julien and M. Massot, *Phys. Chem. Chem. Phys.*, 2002, **4**, 4226–4235.
28 A. C. Ferrari, J. C. Meyer, V. Scardaci, C. Casiraghi, M. Lazzeri, F. Mauri, S. Piscanec, D. Jiang, K. S. Novoselov, S. Roth and A. K. Geim, *Phys. Rev. Lett.*, 2006, **97**, 187401.
29 R. J. Nemanich and S. A. Solin, *Phys. Rev. B: Condens. Matter Mater. Phys.*, 1979, **20**, 392–401.
30 R. P. Vidano, D. B. Fischbach, L. J. Willis and T. M. Loehr, *Solid State Commun.*, 1981, **39**, 341–344.
31 K.-C. Chang, L. Li and E. F. Gloyna, *J. Hazard. Mater.*, 1993, **33**, 51–62.
32 Y. Chen, Y. Zhang, D. Geng, R. Li, H. Hong, J. Chen and X. Sun, *Carbon*, 2011, **49**, 4434–4442.
33 J.-L. Li, K. N. Kudin, M. J. McAllister, R. K. Prud'homme, I. A. Aksay and R. Car, *Phys. Rev. Lett.*, 2006, **96**, 176101.
34 T. K. Gupta, B. P. Singh, S. R. Dhakate, V. N. Singh and R. B. Mathur, *J. Mater. Chem. A*, 2013, **1**, 9138–9149.
35 H.-B. Zhang, Q. Yan, W.-G. Zheng, Z. He and Z.-Z. Yu, *ACS Appl. Mater. Interfaces*, 2011, **3**, 918–924.
36 A. P. Singh, M. Mishra, P. Sambyal, B. K. Gupta, B. P. Singh, A. Chandra and S. K. Dhawan, *J. Mater. Chem. A*, 2014, DOI: 10.1039/c3ta14212d.
37 A. P. Singh, M. Mishra, A. Chandra and S. K. Dhawan, *Nanotechnology*, 2011, **22**, 9.
38 K. Singh, A. Ohlan, V. H. Pham, B. R. S. Varshney, J. Jang, S. H. Hur, W. M. Choi, M. Kumar, S. K. Dhawan, B.-S. Kong and J. S. Chung, *Nanoscale*, 2013, **5**, 2411–2420.
39 A. Ohlan, K. Singh, A. Chandra and S. K. Dhawan, *ACS Appl. Mater. Interfaces*, 2010, **2**, 927–933.
40 X. Sun, J. He, G. Li, J. Tang, T. Wang, Y. Guo and H. Xue, *J. Mater. Chem. C*, 2013, **1**, 765–777.
41 Y. A. Urzhumov, *Sub-wavelength Electromagnetic Phenomena in Plasmonic and Polaritonic Nanostructures: From Optical Magnetism to Super-resolution*, The University of Texas at Austin, 2007.
42 H. Yu, T. Wang, B. Wen, M. Lu, Z. Xu, C. Zhu, Y. Chen, X. Xue, C. Sun and M. Cao, *J. Mater. Chem.*, 2012, **22**, 21679–21685.
43 C. Wang, X. Han, P. Xu, X. Zhang, Y. Du, S. Hu, J. Wang and X. Wang, *Appl. Phys. Lett.*, 2011, **98**, 072906–072903.
44 T. K. Gupta, B. P. Singh, R. B. Mathur and S. R. Dhakate, *Nanoscale*, 2014, **6**, 842–851.
45 X. G. Liu, D. Y. Geng, H. Meng, P. J. Shang and Z. D. Zhang, *Appl. Phys. Lett.*, 2008, **92**, 173117–173113.
46 Y.-F. Zhu, L. Zhang, T. Natsuki, Y.-Q. Fu and Q.-Q. Ni, *ACS Appl. Mater. Interfaces*, 2012, **4**, 2101–2106.
47 M.-S. Cao, J. Yang, W.-L. Song, D.-Q. Zhang, B. Wen, H.-B. Jin, Z.-L. Hou and J. Yuan, *ACS Appl. Mater. Interfaces*, 2012, **4**, 6949–6956.